I&EC research
Industrial & Engineering Chemistry Research

pubs.acs.org/IECR
Article

CO_2-Driven pH Control in the Enzymatic Hydrolysis of Urea: A Coupled Modeling-Experiment Approach

Published as part of Industrial & Engineering Chemistry Research special issue "Smart Reactors - Towards Adaptive, Resilient, and Autonomous Process Systems".

Kayla Reata Dittmer, Leandros Paschalidis,* Chloe Ng-Brossard, Daniel Ohde, Andreas Liese,* and Mirko Skiborowski*

Cite This: https://doi.org/10.1021/acs.iecr.6c00912

ABSTRACT: Enzymatic biotransformations can offer sustainable alternatives to conventional chemical processes, but their activity often strongly depends on the pH of the reaction solution. The urease-catalyzed hydrolysis of urea provides a mild route for ammonia production; however, this ammonia production inherently increases the pH in a buffer-free system, rapidly decreasing urease activity. In this work, we combine modeling and experiments to develop a buffer-free pH control strategy for the enzymatic hydrolysis of urea that relies on the dissolution of gaseous carbon dioxide (CO_2). CO_2, which is actually a byproduct of enzymatic urea hydrolysis, is deliberately added to regulate the pH and enhance productivity. A kinetic model for urea hydrolysis is coupled with a thermodynamic model of the acid−base equilibria in the aqueous phase to analyze and design the process. Bayesian optimization is applied to calculate the optimal partial pressures for CO_2 in the gas phase to maximize productivity. The resulting concept is successfully demonstrated experimentally, highlighting a practical approach with minimal downstreaming requirements to control pH in enzymatic reactions.

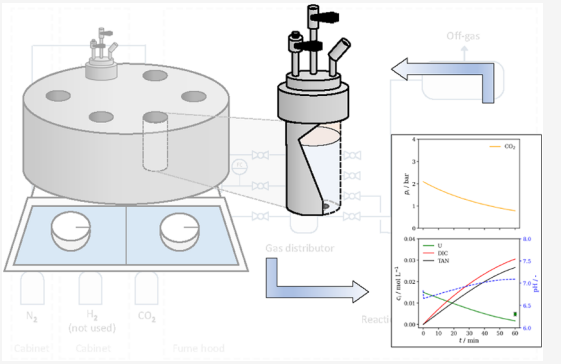

INTRODUCTION

Enzymes have extensive applications in industrial and environmental fields as they enable specific reactions to occur under relatively mild temperature and pressure conditions.[1] Urease (EC 3.5.1.5) is a ubiquitous metalloenzyme found in plants, fungi, algae, bacteria, and invertebrates. It selectively hydrolyzes urea into ammonia (NH_3) and carbon dioxide (CO_2).[2,3] The active site of urease is composed of two Ni(II) ions, four histidines, a carbamylated lysine, and an aspartate residue.[4−6] Urease-based systems have been applied in diverse fields, including medical devices for blood urea removal and dialysate regeneration,[7,8] analytical biosensors for urea detection,[9,10] and environmental processes such as wastewater treatment.[11,12] More recently, urease-catalyzed urea hydrolysis has gained attention as a sustainable route for ammonia production from urine, offering a potential low-energy complement to the Haber-Bosch process.[13,14]

Urease activity is strongly dependent on the solution pH, reaching its maximum at around pH 7 and decreasing under more acidic or alkaline conditions.[15] In a buffer-free system, the pH of the urea hydrolysis reaction often increases to a plateau of about 9, where the self-buffering effect of an ammonia-ammonium buffer takes effect.[16] At this pH, the enzyme activity decreases significantly; therefore, pH control can enhance productivity by maintaining the pH in a favorable range, maximizing activity. However, pH control through buffer salts often poses a challenge due to the need for product purification and possible difficulties in downstream processes. Developing buffer-reduced or buffer-free process strategies, therefore, contributes to more resource-efficient and environmentally compatible biocatalytic systems. These aspects directly reflect the activities of the United Nations University (UNU) Hub at the Hamburg University of Technology (TUHH), which focuses on translating sustainability goals into technological solutions for industrial biotechnology. The work supports Sustainable Development Goal (SDG) 12, "Responsible Consumption and Production", by decreasing material use and process waste, and SDG 9, "Industry, Innovation and Infrastructure", by developing innovative and more sustainable bioprocess engineering strategies that can be integrated into future industrial applications.

Received: March 3, 2026
Revised: May 23, 2026
Accepted: May 26, 2026

https://doi.org/10.1021/acs.iecr.6c00912
Ind. Eng. Chem. Res. XXXX, XXX, XXX−XXX

While CO_2 is a byproduct of the reaction, its exogenous addition can counteract the predominant basicity arising from the ammonium-ammonia equilibrium, thus offering a potential method for pH control in the enzymatic hydrolysis of urea. Consequently, we propose deliberately adding gaseous CO_2 to the reactor to offset the increase in basicity caused by the stoichiometry of the hydrolysis reaction. This approach eliminates the need for additional salts, simplifying the reaction setup and reducing its environmental impact,[17] and is not entirely unprecedented. For example, Hoshan et al.[18] demonstrated precise pH control in CHO cell cultures via feedback adjustment of air/CO_2 ratios in the sparging gas, thus avoiding base addition. Similarly, Xu and Chen[19] achieved high-density mammalian cell cultures by optimizing the dissolved CO_2 concentration.

This work aims to demonstrate the applicability of such a gaseous CO_2-driven pH control in the enzymatic hydrolysis of urea. Such a method allows pH control with minimum downstream requirements, using a byproduct of the same process, and can therefore help eliminate costs that would arise from the use of buffers. Nevertheless, in a pilot scale, the implementation of pressurized reactors with CO_2 as a pH regulator may add complexity to reactor design. A combined modeling and experimental approach is adopted. In recent years, the design of enzymatic systems guided by kinetic models has received considerable attention.[20−23] Despite the availability of kinetic models for urease-catalyzed urea hydrolysis,[15,16,24,25] limited research has focused on integrating these models with pH control and experimental validation of model-based design. Although prior studies have separately addressed urease kinetics and CO_2-assisted pH control, there is a research gap regarding an integrative approach combining specifically kinetic modeling with thermodynamic and mass transfer considerations for enzymatic urea hydrolysis under CO_2 overpressure. The kinetic model developed by Fidaleo and Lavecchia[25] is adopted from the literature and combined with a thermodynamic model of the resulting aqueous acid−base equilibria[26] and interfacial gas−liquid mass transfer. The model is used to gain insight into the reaction process. It is fitted and validated against experimental data, as well as used to select the conditions of the reaction process, selected by means of a Bayesian optimization approach to maximize productivity by selecting the optimal initial CO_2 partial pressure. The results demonstrate CO_2 addition to be a viable strategy for pH control in the enzymatic hydrolysis of urea.

MATERIALS AND METHODS

The Enzymatic Hydrolysis of Urea

The hydrolysis of urea is a key reaction in many industrial and environmental systems, particularly in wastewater treatment, fertilizer management, and emission control technologies.[11,12] The reaction converts urea into ammonia and CO_2 according to

$$(NH_2)_2CO + H_2O \xrightarrow{\text{urease}} 2NH_3 + CO_2 \quad (1)$$

In aqueous systems, the released ammonia participates in the ammonia-ammonium acid−base equilibrium, increasing the pH. The generated CO_2 equilibrates with water to form carbonic acid, which partially dissociates to bicarbonate and carbonate. From a process-engineering standpoint, these equilibria must be considered when designing reactors, scrubbers, or biological treatment units, as they directly affect pH, mass transfer rates, and off-gas composition. Accurate modeling requires the inclusion of all aqueous equilibria, gas−liquid mass transfer of NH_3 and CO_2, and potential pH feedback effects that influence reaction kinetics and speciation. The acid−base equilibria present are described below.

$$NH_3 + H_2O \rightleftharpoons NH_4^+ + OH^- \quad (2)$$

$$CO_{2(aq)} + H_2O \rightleftharpoons H_2CO_3 \quad (3)$$

$$H_2CO_3 \rightleftharpoons H^+ + HCO_3^- \quad (4)$$

$$HCO_3^- \rightleftharpoons H^+ + CO_3^{2-} \quad (5)$$

$$H_2O \rightleftharpoons H^+ + OH^- \quad (6)$$

If ammonium carbamate forms transiently, then the following reactions must also be included.

$$(NH_2)_2CO + H_2O \rightleftharpoons NH_4^+ + NH_2COO^- \quad (7)$$

$$NH_2COO^- + H_2O \rightleftharpoons NH_3 + HCO_3^- \quad (8)$$

In this work, the last two reactions were omitted, as ammonium carbamate is a short-lived intermediate that does not accumulate appreciably under the dilute, near-ambient conditions considered here, and its rapid hydrolysis means the overall stoichiometry is well represented by the direct formation of ammonia and CO_2.[26]

KINETIC MODEL

The reaction kinetics adopted in this work are based on the mechanistic model reported by Fidaleo and Lavecchia,[25] who described enzymatic urea hydrolysis using a modified Michaelis−Menten expression including pH dependence and noncompetitive product inhibition. A single-substrate kinetic formulation is assumed because water is present in large excess and its concentration remains effectively constant throughout the reaction, such that its influence is incorporated into the apparent kinetic parameters and does not need to be treated explicitly as a second substrate. Apart from the pH dependency and noncompetitive product inhibition, the activity of the enzyme is assumed to be constant throughout the reaction process. The reaction rate is expressed as

$$r = \exp\left[-\frac{E_a}{R}\left(\frac{1}{T} - \frac{1}{T^*}\right)\right]\frac{c_E c_U}{\left(1 + (c_{NH_3}/K_P)\right)(K_M + c_U)} f_{pH} \quad (9)$$

where the pH-dependent activity factor is given by

$$f_{pH} = \frac{1}{1 + \frac{10^{-pH}}{K_{ES,1}} + \frac{K_{ES,2}}{10^{-pH}}} \quad (10)$$

In the above expressions, r denotes the volumetric reaction rate. E_a is the apparent activation energy, R the universal gas constant, T the absolute temperature, and T^* the reference temperature (414.6 K) representing the temperature at which the kinetic constant equals 1 mol g^{-1} min^{-1}.[25] The terms c_E and c_U represent the concentrations of active enzyme and urea, respectively. K_M is the Michaelis constant (assumed to be independent of the pH in this model in accordance with the work of Fidaleo and Lavecchia[25]), while K_P denotes the product inhibition constant. c_{NH_3} corresponds to the concentration of ammonia. The factor f_{pH} accounts for the pH-dependent enzyme activity. $K_{ES,1}$ and $K_{ES,2}$ are apparent equilibrium constants describing protonation and deprotonation equilibria of the enzyme−substrate complex, and pH is defined as $-\log_{10}(c_{H^+})$. This formulation accounts for:

- Michaelis−Menten substrate dependence
- Product inhibition

https://doi.org/10.1021/acs.iecr.6c00912
Ind. Eng. Chem. Res. XXXX, XXX, XXX−XXX

- pH-dependent enzyme activity
- Arrhenius-type temperature dependence of the rate coefficient

It should be noted that the original expression proposed by Fidaleo and Lavecchia[25] attributes noncompetitive inhibition to ammonium ions, while considering ammonium and bicarbonate ions as reaction products. In the present work, however, the inhibition term is formulated as a function of ammonia concentration. This is done solely for consistency with the adopted reaction stoichiometry (where ammonia is considered as the reaction product) and does not imply any change in the underlying assumption of ammonium-based inhibition proposed by Fidaleo and Lavecchia;[25] due to the rapid acid−base equilibrium between NH_3 and NH_4^+, their relative concentrations are uniquely determined by pH, such that the use of NH_3 leads to an apparent inhibition constant that implicitly accounts for equilibrium speciation effects. The model is thus used as a semiempirical kinetic expression suitable for process modeling and design, rather than a detailed mechanistic description of enzyme inhibition. The kinetic parameters and units used in the model are reported in Table 1.

Table 1. Kinetic Parameters for Enzymatic Urea Hydrolysis

parameter	value	units
K_M	3.21×10^{-3}	mol L^{-1}
$K_{ES,1}$	7.57×10^{-7}	mol L^{-1}
$K_{ES,2}$	1.27×10^{-8}	mol L^{-1}
K_P	1.22×10^{-2}	mol L^{-1}
E_a	35.3×10^{3}	J mol^{-1}
T^*	414.6	K

These parameter values were obtained by nonlinear regression of initial-rate experimental data as described by Fidaleo and Lavecchia.[25] To adjust the kinetic model to the urease powder used in this work, an additional parameter f_{ac} was multiplied to the numerator, adjusting the enzyme activity per gram of the powder. This parameter was fitted to experimental data from this work, cf. Section model parametrization.

Acid−Base Equilibria Model

The pH of the aqueous solution containing ammonia and inorganic carbon species was calculated based on the principle of *electroneutrality* and the dissociation equilibrium constants of relevant species as functions of temperature, using the methodology reported by Petersen et al.[26] The temperature-dependent equilibrium constants for the relevant reactions were computed using the following empirical formulas

$$K_{NH_3} = e^{\left(191.97 - \frac{8451.61}{T} - 31.4335 \ln T + 0.0152123T\right)} \quad (11)$$

$$K_{CO_2} = e^{\left(2767.92 - \frac{80063.5}{T} - 478.653 \ln T + 0.714984T\right)} \quad (12)$$

$$K_{HCO_3^-} = e^{\left(12.405 - \frac{6286.89}{T} - 0.050628T\right)} \quad (13)$$

$$K_{H_2O} = e^{\left(14.01708 - \frac{10294.83}{T} - 0.039282T\right)} \quad (14)$$

Here, K_{NH_3}, K_{CO_2}, $K_{HCO_3^-}$, and K_{H_2O} correspond to the dissociation equilibrium constants of ammonia, CO_2, bicarbonate, and water, respectively. The hydronium ion concentration $[H^+]$ was determined by solving the electroneutrality condition. The principle of electroneutrality states that any macroscopic solution must be electrically neutral, meaning that the total positive charge equals the total negative charge. In aqueous systems, this implies that the sum of all cation concentrations (e.g., H^+, NH_4^+) must equal the sum of all anion concentrations (e.g., OH^-, HCO_3^-, CO_3^{2-}). The electroneutrality is used to solve for unknown concentrations, such as the proton concentration, ensuring that charge balance is maintained throughout the system, as shown below

$$c_{H^+} = -c_{NH_4^+} + c_{HCO_3^-} + 2c_{CO_3^{2-}} + c_{OH^-} \quad (15)$$

The species concentrations were calculated as fractions of the total ammonia nitrogen (TAN) and dissolved inorganic carbon (DIC)

$$c_{NH_4^+} = \alpha_{NH_4} c_{TAN} \quad (16)$$

$$c_{NH_3} = \alpha_{NH_3} c_{TAN} \quad (17)$$

$$c_{HCO_3^-} = \alpha_{HCO_3} c_{DIC} \quad (18)$$

$$c_{CO_3^{2-}} = \alpha_{CO_3} c_{DIC} \quad (19)$$

$$c_{CO_{2(aq)}} = \alpha_{CO_2} c_{DIC} \quad (20)$$

$$K_{H_2O} = c_{H^+} c_{OH^-} \quad (21)$$

where the fractions α_i are derived from the equilibrium constants and the hydronium concentration

$$\alpha_{NH_3} = \frac{K_{H_2O}}{K_{H_2O} + K_{NH_3} c_{H^+}} \quad (22)$$

$$\alpha_{NH_4} = \frac{K_{NH_3} c_{H^+}}{K_{NH_3} c_{H^+} + K_{H_2O}} \quad (23)$$

$$\alpha_{CO_2} = \frac{c_{H^+}^2}{c_{H^+}^2 + K_{CO_2} c_{H^+} + K_{CO_2} K_{HCO_3^-}} \quad (24)$$

$$\alpha_{HCO_3} = \frac{K_{CO_2} c_{H^+}}{c_{H^+}^2 + K_{CO_2} c_{H^+} + K_{CO_2} K_{HCO_3^-}} \quad (25)$$

$$\alpha_{CO_3} = \frac{K_{CO_2} K_{HCO_3^-}}{c_{H^+}^2 + K_{CO_2} c_{H^+} + K_{CO_2} K_{HCO_3^-}} \quad (26)$$

The hydronium concentration c_{H^+} was obtained numerically using a root-finding algorithm to satisfy the electroneutrality condition. The solution was then converted to pH

$$pH = -\log_{10}(c_{H^+}) \quad (27)$$

Calculations were performed over a range of TAN and DIC values to produce a contour map of pH as a function of solution composition (Figure 4).

Gas−Liquid Mass Transfer Model

The applied gas−liquid mass transfer model describes the change in partitioning of ammonia and CO_2 between the liquid and gas phases. The liquid phase was considered ideal, with temperature-dependent equilibrium constants determining the aqueous speciation. The gas phase was assumed to be ideal, with partial pressures given by

https://doi.org/10.1021/acs.iecr.6c00912
Ind. Eng. Chem. Res. XXXX, XXX, XXX−XXX

$$p_i = \frac{n_{i,g} RT}{V_{gas}} \tag{28}$$

where n_i is the moles of component i, R is the universal gas constant, T is the temperature, and V_{gas} is the gas volume. Gas−liquid mass transfer was modeled as follows

$$j_{i,transfer} = k_L a(c_i - H_i p_i) \tag{29}$$

where $k_L a$ is the effective volumetric mass transfer coefficient and H_i is Henry's law constant. The gas−liquid mass transfer model was coupled to the electroneutrality constraint in the liquid phase to determine pH dynamically.

Reactor Model and Main Assumptions

The reactor was modeled as an ideally mixed, isothermal batch system with fixed liquid and gas volumes. The time-dependent material balances for key species are

$$\frac{dc_U}{dt} = -r_e \tag{30}$$

$$\frac{dc_{TAN}}{dt} = 2r_e - j_{NH_3,transfer} \tag{31}$$

$$\frac{dc_{DIC}}{dt} = r_e - j_{CO_2,transfer} \tag{32}$$

$$\frac{dn_{NH_3,g}}{dt} = j_{NH_3,transfer} V_{liq} \tag{33}$$

$$\frac{dn_{CO_2,g}}{dt} = j_{CO_2,transfer} V_{liq} \tag{34}$$

Here, r is the reaction rate of the enzymatic hydrolysis reaction in eq 9 and j are the mass transfer rates according to eq 29. Gas-phase transfer rates are represented as described above. The dissociation of the main species to other species in the liquid phase or the gas phase are determined by the acid−base model and Henry's law, respectively. The main assumptions applied are listed below:

- Isothermal operation:
- Perfect mixing occurs in both liquid and gas phases.
- Ideal gas behavior for NH_3 and CO_2 in the headspace.
- Electroneutrality in the liquid phase was used to determine pH dynamically.
- The acid−base equilibria are considered instantaneous,[27,28] while the rate of the enzymatic reaction is considered to follow kinetics described by the semi-empirical kinetic model.

Numerical Implementation and Solution Strategy

The model was implemented in Python to solve the coupled differential equations governing hydrolysis, aqueous speciation, and gas−liquid mass transfer. The system state is described by five variables: urea concentration, TAN, DIC, and the moles of ammonia and carbon dioxide in the gas phase. At each time step, the solution pH is obtained by solving the charge balance (electroneutrality) condition for the aqueous phase, which accounts for all relevant acid−base equilibria, including NH_3/NH_4^+, $CO_2/HCO_3^-/CO_3^{2-}$, and water autoionization. Equilibrium constants are evaluated at a fixed temperature (308.15 K) using the temperature-dependent expressions. The system of coupled differential equations was solved using the implicit BDF method (solve ivp, SciPy) with relative and absolute tolerances of 10^{-6} and 10^{-9}, respectively, while pH was computed at each time step via a Brent root-finding algorithm. The root-finding algorithm robustly identifies the hydrogen ion concentration (pH) satisfying the electroneutrality constraint over the interval $2 \le pH \le 12$ for given values of TAN and DIC.

The kinetics of the urease-catalyzed urea hydrolysis is incorporated via the presented rate expression and the corresponding material balances. Mass transfer between the liquid and gas phases for CO_2 and NH_3 is modeled using overall mass transfer coefficients ($k_L a$) and Henry's law to relate aqueous concentrations to gas phase partial pressures. The full set of ordinary differential equations is integrated in time using a stiff integrator (scipy.integrate.solve_ivp with the backward differentiation formula (BDF) method), which handles the disparate time scales introduced by rapid chemical equilibria and slower kinetic processes.

Optimization Methodology

To identify optimal initial conditions that minimize the residual urea concentration after a fixed reaction time, we embedded the reactor model in a probabilistic global optimization framework. The underlying problem is to minimize the resulting urea concentration after 60 min, based on the initial CO_2 partial pressure

$$\min c_U(60\ \text{min}) \tag{35}$$

It is particularly challenging to solve due to numerically integrating a stiff system of ordinary differential equations that includes iterative root-finding to compute the solution pH from TAN and DIC. Since there is no closed-form expression for the pH dependency and the pH solver (Brent's method) introduces inherently nonsmooth behavior, the resulting objective function is effectively a *black-box* with respect to the optimization variables and can be expensive computationally to evaluate.

Given this, a derivative-free Bayesian optimization approach was selected and implemented via the gp_minimize algorithm rather than a classical gradient-based nonlinear programming (NLP) solver. The optimization of the initial CO_2 pressure was performed using Bayesian optimization (`gp_minimize`, `scikit-optimize`) over a bounded search space (0−3.5 atm), using an Expected Improvement acquisition function and a fixed random seed to ensure reproducibility. A key motivation for using Bayesian optimization in this work is the difficulty that traditional NLP solvers such as IPOPT face with this problem class. Standard NLP methods rely on gradient information and smooth, differentiable objective and constraint functions; however, the nested pH calculation in our model is based on a root-finding procedure that introduces discontinuities and nonanalytic behavior with respect to the decision variables. Such behavior can confound gradient estimates, lead to poor convergence, and trap solvers in local minima. By contrast, Bayesian optimization treats the simulation model as a true black box and does not require gradients, circumventing the need for differentiability and making it less sensitive to the tricky equilibrium and pH calculations inherent in multiphase, multiphysics systems of the type considered here. All relevant code is provided online in a link at the end of the paper.

Materials

Urea (≥99.5% p. a.) and ammonium chloride (NH_4Cl; ≥ 99.5% p. a.) were purchased from Carl Roth GmbH + Co. KG

https://doi.org/10.1021/acs.iecr.6c00912
Ind. Eng. Chem. Res. XXXX, XXX, XXX−XXX

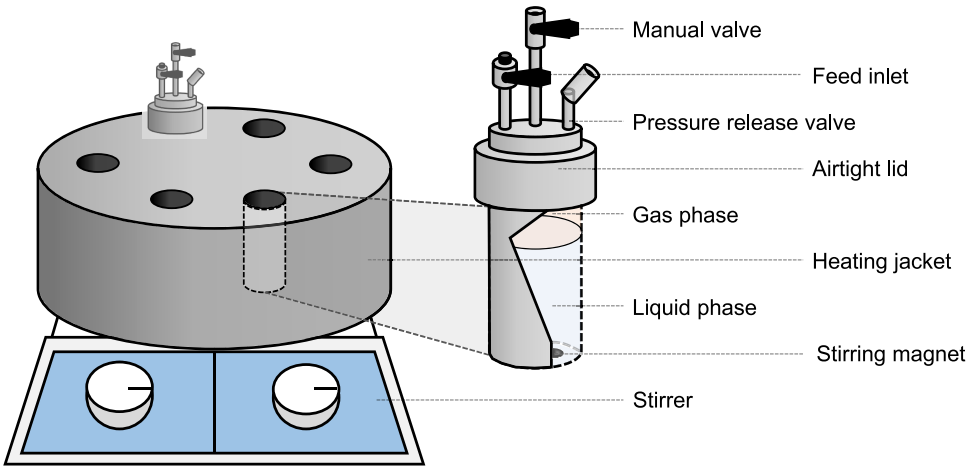

Figure 1. Schematic diagram of the experimental setup. The aluminum block on the magnetic stirrer has six inlets for each reactor for tempering and stirring. Each reactor has a lid with two manual valves and a pressure release valve.

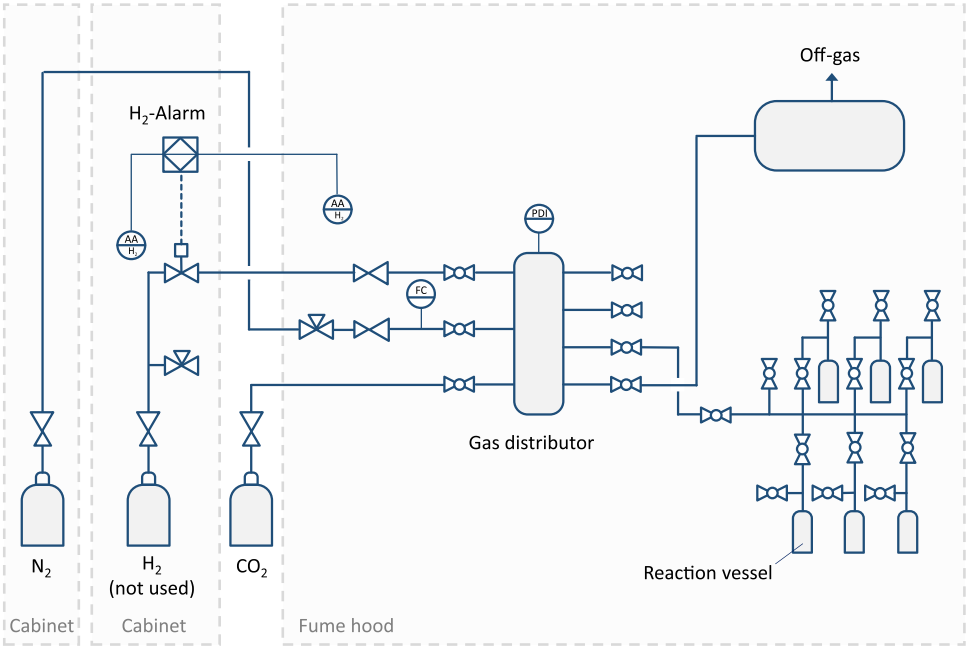

Figure 2. Process flow diagram of the gas distribution system used for parallel reactor pressurization as described and used in Schlipköter et al.[29]

(Karlsruhe, Germany). Gas bottles of CO_2 (99.995%, 4.5 grade) and N_2 (99.99%, 5 grade) were obtained from Westfalen AG (Münster, Germany). HPLC columns were supplied by Bischoff Analysentechnik u. -geräte GmbH (Leonberg, Germany). Urease from *Canavalia ensiformis* (Type IX; Jack bean) with 90.76 U/mg (1 μmol ammonia per minute at pH 7 and 25 °C) was purchased from Merck Sigma-Aldrich (St. Louis, MO, USA). ACR011 Orion AQUAfast ammonia test kits were obtained from Thermo Fisher Scientific Inc. (Waltham, MA, USA).

Experimental Setup

Custom-built 20 mL pressurizable reactors developed by the Chair of Technical Chemistry at the Technical University of Dortmund, as seen in Figure 1 were used for all experiments.[29] Each reactor lid was equipped with a pressure release valve (70 bar ± 10%) and two manual valves, allowing simultaneous pressurization of up to six reactors via a gas distributor, as seen in the process flow diagram (PFD) in Figure 2.

150 μL urease solution (2.5 g/L) was pipetted into each reactor. Magnetic stirring bars were added, and the reactor lids were securely screwed on. The reaction vessels were mounted onto a frame connected to a gas distributor, which enables controlled gas supply to each reactor and pressure monitoring via a barometer. First, air-tightness was verified by pressurizing the system with N_2 to 2 bar; stable pressure for at least 5 min confirmed hermetic sealing. 0.030 M urea solution was prepared in Milli-Q water and sparged with humidified N_2 gas at 100 mL/min until dissolved CO_2 was removed and the initial pH of the solution reached 7. The pH of the urea solution was measured using a PCE-228 pH meter (PCE Instruments UK Ltd., Southampton, United Kingdom). Next, 15 mL urea solution (5 mL headspace) was injected into each reactor through the feed valve.

While all inlet valves of the reaction vessels were closed, the CO_2 pressure was adjusted. Once the desired pressure was reached, the inlet valves of the respective reactors were opened to pressurize the reactors. After pressurizing, the inlet valves

https://doi.org/10.1021/acs.iecr.6c00912
Ind. Eng. Chem. Res. XXXX, XXX, XXX−XXX

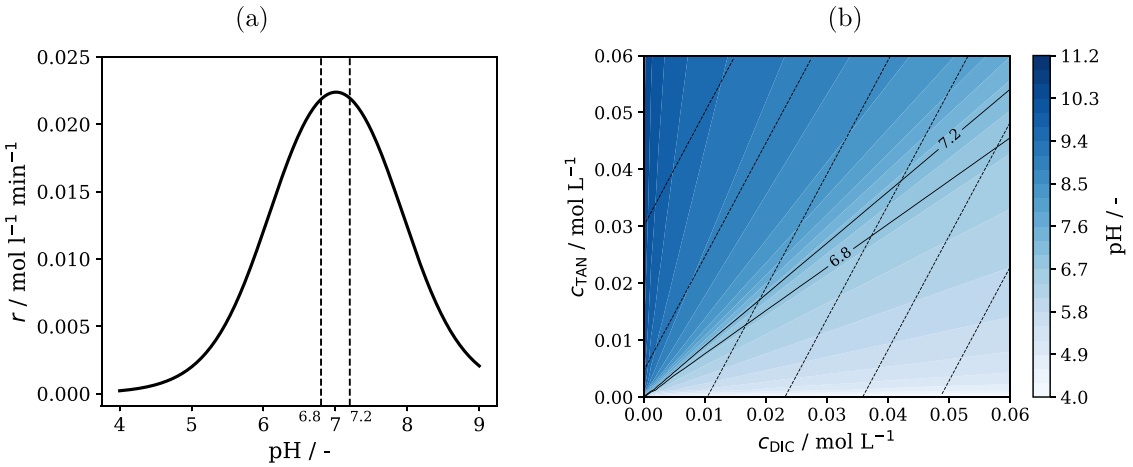

Figure 3. Model results describing pH-dependent system behavior. The lines at pH 6.8 and 7.2 show the optimal pH region. (a) Predicted reaction rate of the urea hydrolysis for 1 g/L of enzyme under substrate saturation conditions and with no product present. (b) Calculated pH values as a function of TAN and DIC concentrations at 35 °C.

were once again closed, thus maintaining the desired pressure in the reactor. This was done with each reactor for the corresponding pressures. Before dismounting the reactors, the off-gas valve in the gas distributor was opened to release the pressure. Once removed from the frame, the reactors were temperature controlled by placing them on an aluminum block with an inlet for a temperature controller and six inlets corresponding to each reactor (Figure 1). The aluminum block was heated using a magnetic heating plate with temperature control (Heidolph Scientific Products GmbH, Schwabach, Germany), which enabled continuous stirring while maintaining a constant temperature in each reactor. The reaction temperature was maintained at 35 °C with a stirring speed of 500 rpm.

After 60 min of reaction time, the reactors were carefully depressurized and opened. Immediately after opening the reactor, the pH was measured. A 1 mL reaction sample was withdrawn from each reactor and transferred into 1.5 mL SafeSeal reaction tubes (Sarstedt AG & Co. KG, Nümbrecht, Germany). The tubes were sealed and placed on a PCMT Thermoshaker (Grant Instruments Ltd., Cambridge, United Kingdom) at 90 °C and 500 rpm for 15 min to thermally deactivate the enzyme. The temperature was maintained below boiling to prevent the caps from opening due to vapor pressure. After heating, the samples were cooled on ice and vortexed to ensure a uniform composition. All experiments were carried out in triplicate, and results are reported as mean ± standard deviation.

Analytical Methods

Two offline analytical methods were carried out for the reaction characterization. For high-performance liquid chromatography (HPLC) sample preparation, 600 μL of the samples were filtered through Rotilabo regenerated cellulose (RC) syringe filters (0.2 μm pore size, 15 mm diameter; Carl Roth GmbH + Co. KG, Karlsruhe, Germany). To prevent bubble formation in the HPLC column, samples were sparged with humidified N_2 for 2 min at 10 mL/min prior to injection. The HPLC method was based on the urea analysis described in Microsolv.[30] Separations were performed using a Prontosil C18 AQ column (250 × 4.0 mm i.d., 10 μm particle size, 120 Å pore size) on an Agilent 1100 HPLC system (Agilent Technologies, Waldbronn, Germany). A similar C18 guard column (30 mm length, 5 μm particle diameter) was installed upstream to protect the analytical column from potential contaminants. Both columns contained a nonpolar C18 stationary phase and were operated under reversed-phase conditions. Milli-Q water served as an eluent, and the flow rate was set to 0.5 mL/min. The sampling volume was 20 μL. Urea was detected at a wavelength of 200 nm. Ammonia and carbonate solutions displayed no interference with the urea peaks. The retention time of urea was 5.54 min. The limit of detection (LOD), calculated from the calibration curve (as seen in Tables S2 and S3 in the Supporting Information), was established at 1.77 mM, and the limit of quantitation (LOQ) was determined to be 5.37 mM. The second analytical method was the implementation of ammonia test kits, applied following the manufacturer's protocol based on the salicylate method. The reaction samples were diluted 1:25 to be within the quantification range of the kit (1−50 mg/L NH_4−N). The calibration curve was performed by a dilution series from an NH_4Cl stock solution measured at 660 nm in a T00 PRO microplate reader (Tecan, Männedorf, Switzerland). Calibration curves for the urea (HPLC) and ammonia (test kit) are displayed in the SI.

RESULTS AND DISCUSSION

The Role of pH

Using the reaction rate model, the influence of pH on enzymatic activity was quantified. Figure 3a shows the predicted reaction rate for an enzyme concentration of 1 g L^{-1} under substrate-saturated conditions with no product inhibition (the activity correction parameter, f_{ac} is also not used for these preliminary calculations). The results exhibit a pronounced dependence of the reaction rate on pH: the rate reaches a maximum near neutral pH (≈ 7), whereas at pH 9 the predicted rate is substantially lower, approximately an order of magnitude below the optimum. This pronounced pH sensitivity underscores the importance of accurate pH control when designing and optimizing urease-catalyzed processes.

By decoupling the acid−base equilibria from the reaction kinetics, the pH of the system was calculated as a function of the TAN and DIC. The calculation was performed for 35 °C, and the results are presented in Figure 3b. Figure 3b shows the pH for different DIC and TAN concentrations. The black lines

https://doi.org/10.1021/acs.iecr.6c00912
Ind. Eng. Chem. Res. XXXX, XXX, XXX−XXX

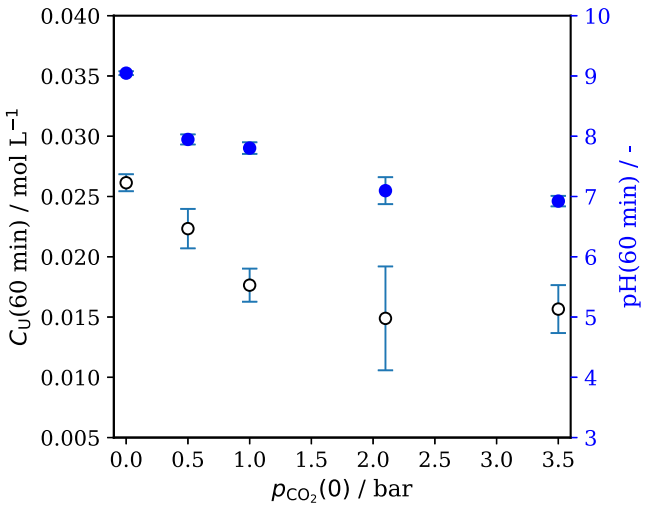

Figure 4. Dependency of final urea concentration and pH after a 60 min reaction time on the CO_2 overpressure in the reactor. Reaction conditions: 0.030 M initial urea concentration, 15 mL reaction solution, 25 mg/L urease powder, 5 mL headspace at 35 °C with 500 rpm stirring. Results are shown as mean ± standard deviation of experimental triplicates (n = 3). Model-experimental comparisons are given in parity plots in Figures S21 and S22 in the Supporting Information.

Table 2. Estimated Model Parameters and 95% Confidence Intervals

symbol	unit	best fit
k_La	min^{-1}	0.0092 ± 0.0032
f_{ac}		40.0434 ± 6.3643

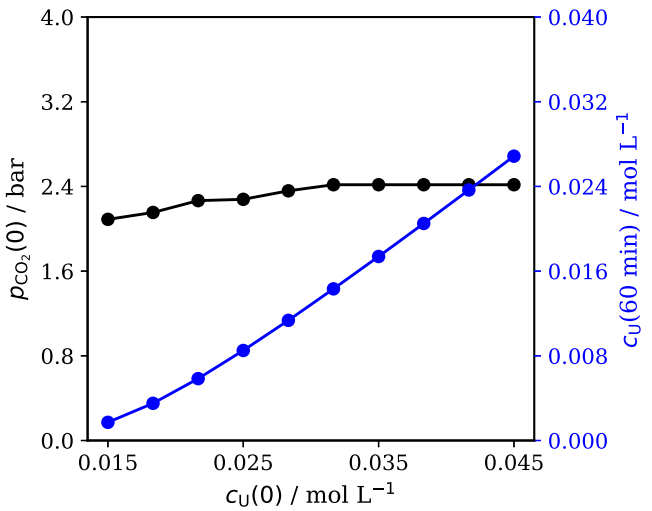

Figure 5. Bayesian optimization results showing the optimal initial CO_2 pressure ($p_{CO_2}(0)$) and the resulting urea concentration after 60 min (c_u(60 min)) for different initial urea concentrations ($c_u(0)$).

indicate a small interval around the optimal pH of approximately 7, for which the activity is close to the maximum (cf. Figure 3a), while the black dashed lines represent the stoichiometric trajectory of urea hydrolysis (2 mol of TAN for every mole of DIC produced), assuming no escape of species from the liquid phase.

The considerable difference in the slopes clearly shows that, independent of the initial composition, the reaction trajectory rapidly deviates from the optimal pH range. As indicated in Figure 3, the reaction rates quickly decrease when deviating from this optimal range, dropping more than 25% when the pH is 7 or 8. This underscores the necessity of active pH control to maintain the enzymatic efficiency. The steep slope of the hydrolysis trajectory can be moderated by the controlled addition of CO_2, enabling the process to be maintained within the desired pH region throughout the reaction.

Experimental Results

The analytical methods used for urea quantification by HPLC and for ammonia determination using commercial ammonia test kits were compared. HPLC data and chromatograms are displayed in the Supporting Information in Table S6 and Figures S5−S19, respectively. When no or little CO_2 is added, the experimental results obtained by both methods are in good agreement. For the experiments with no additional CO_2, the HPLC and ammonia test kit resulted in a final urea concentration of 26.7 ± 1.9 and 26.1 ± 0.7 mM, respectively. However, upon the addition of CO_2 to the system, the HPLC chromatograms exhibited less consistent baselines, which complicated reliable quantification. Due to the technical challenges in the HPLC under elevated CO_2 conditions, the ammonia test kit was selected as the method for urea quantification in this study.

The conversion of urea at different CO_2 pressures was investigated experimentally. In Figure 4, the final urea concentrations of the reaction solution after 60 min of reaction are displayed based on how much CO_2 overpressure was applied. The results demonstrate that even a small addition of CO_2 improves the conversion of urea. These results are in accordance with the literature, which states that urease is activated with CO_2 due to the carbamylation of the lysine residue in the active site, forming a carbamate group.[31] Maithani et al. found that urease activates by linking with specifically $^{12}CO_2$ isotopes.[32] For context, a conventional phosphate-buffered reference paper was considered alongside the present buffer-free CO_2-controlled system. Previous work by Krajewska and Zaborska[33] on jack bean urease showed that phosphate buffer acts as a competitive inhibitor between pH 5.80 and 7.49, which means that pH control by buffering may come at the cost of reduced enzymatic performance. In contrast, the CO_2-based strategy regulates pH without introducing additional buffer components, thereby avoiding this inhibitory effect and supporting a simpler process design.[33]

As expected, the increase in the CO_2 pressure is accompanied by a gradual decrease in pH due to the formation of carbonic acid. The observed changes in urea hydrolysis correlate with this pH shift by influencing the reaction performance via its impact on the reaction pH.

Model Parameterization

The dynamic model contains two parameters that were not known a priori and, therefore, required estimation from experimental data: the effective overall gas−liquid volumetric mass transfer coefficient (k_La) and an activity correction factor (f_{ac}) for the lyophilized urease powder. These parameters were fitted to the experimental concentration profiles shown in Figure 4 using nonlinear regression, implemented via a least-squares minimization of the residuals between model predictions and measured values for the final urea concentrations. The mass transfer coefficient and kinetic factors are adjusted so that the model predictions best match the measured values. This is achieved by minimizing the sum of

https://doi.org/10.1021/acs.iecr.6c00912
Ind. Eng. Chem. Res. XXXX, XXX, XXX−XXX

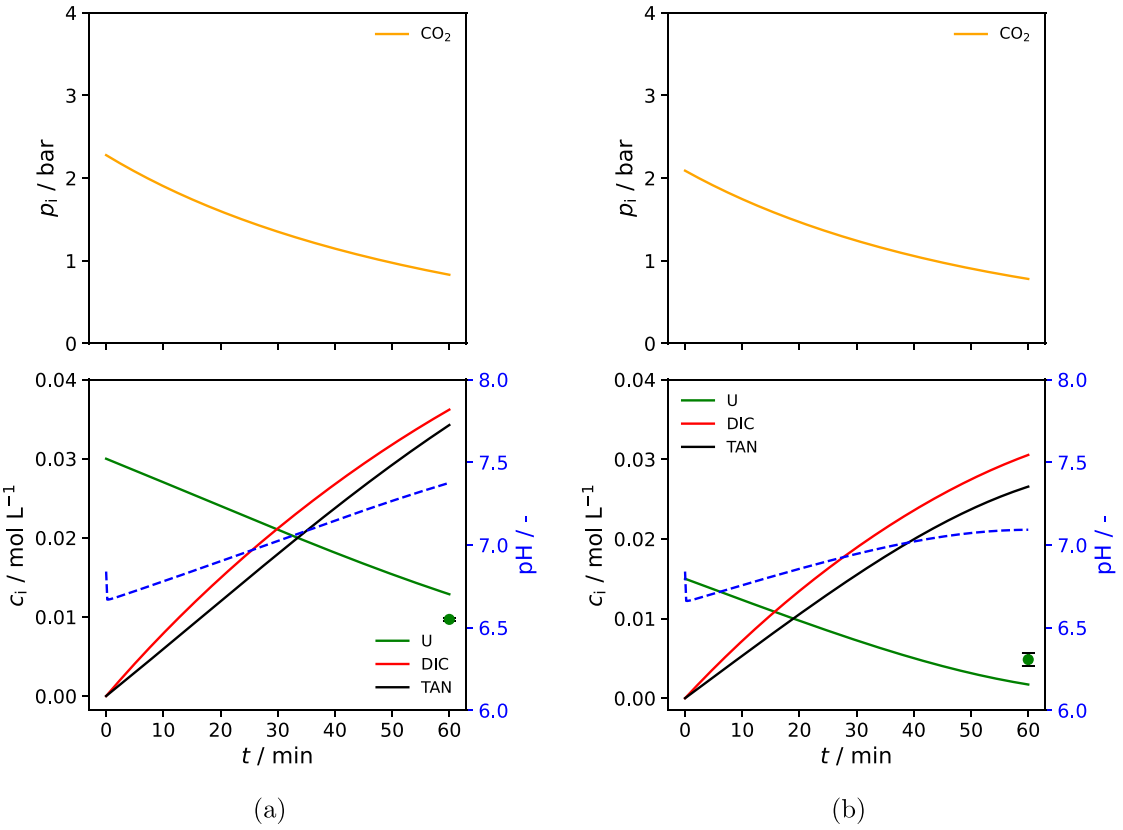

Figure 6. Simulation plots of the Bayesian optimization for urea concentrations at (a) 0.030 M and (b) 0.015 M urea. The green data points represent the experimental results at these conditions. Reaction conditions: 0.030 M initial urea concentration, 15 mL reaction solution, 25 mg/L urease powder, 5 mL headspace at 35 °C with 500 rpm stirring. Results are shown as mean ± standard deviation of experimental triplicates (n = 3).

squared residuals, that is, the differences between simulated and experimental results, using an optimization algorithm. Because the model is nonlinear and involves the solution of differential equations, the parameters are determined iteratively. To assess the quality of the fit, we report an adjusted coefficient of determination of R^2 = 0.90. Parity plots comparing simulated and measured data, as well as the confidence ellipsoid for the joint parameter estimates, are presented in the Supporting Information (Figures S20−S22). The best-fit values and their 95% confidence intervals are given in Table 2.

The nonlinear regression (NLR) method is used to estimate unknown model parameters by fitting a nonlinear model to the experimental data. In this approach, parameters such as Additionally, the Jacobian of the residuals is used to evaluate parameter uncertainty and compute confidence intervals, providing a measure of the reliability of the estimated parameters.

Validation and Model-Based Design

The kinetic model was employed to determine the optimal initial CO_2 partial pressures for the different initial urea concentrations. Bayesian optimization was used to iterate across these initial urea concentrations and calculate the corresponding optimal CO_2 partial pressure. The results are presented in Figure 5, which illustrates the optimal initial CO_2 pressure ($p_{CO_2}(0)$) and the resulting urea concentration after 60 min (c_u(60 min)) for different initial urea concentrations ($c_u(0)$).

Two notable points from the optimization, as reflected in Figure 5, were subsequently tested experimentally, one for 0.015 M and one for 0.030 M initial urea concentration, shown with the simulation results in Figure 6a,6b. The individual results of the Bayesian optimization for these points are illustrated in more detail in Figures S23 and S24 in the Supporting Information, highlighting the respective minimum for the resulting urea concentration after 60 min (c_u(60 min)) in dependence on the initial CO_2 pressure ($p_{CO_2}(0)$). The progress curve plots resulting from the simulation with the optimal initial CO_2 pressure ($p_{CO_2}(0)$) and the experimentally determined values for these values of the urea concentration after 60 min (c_u(60 min)) are shown in Figure 6a,6b, respectively. This experimental validation demonstrated a good prediction of the experimental results, with the model providing further insights into the temporal development of the species concentrations and changes in pH.

Overall, the model demonstrated good predictive capability and proved to be useful for analyzing, understanding, and designing the reaction processes. Particularly, the effective exploitation of CO_2 partial pressure to control pH and improve productivity could be validated and provides further potential for optimal process control by means of a temporal adjustment of the pH via CO_2 dosing. Despite the good performance of the model, variations in enzyme activity between different enzyme batches, combined with the dependence of the volumetric mass transfer coefficient (k_La) on the geometry and stirring or sparging conditions of the specific setup, make these two parameters critical for performance prediction and require an accurate estimation when designing such systems.

https://doi.org/10.1021/acs.iecr.6c00912
Ind. Eng. Chem. Res. XXXX, XXX, XXX−XXX

These uncertainties, furthermore, create additional challenges that need to be tackled when pursuing model-based process control.

CONCLUSION

This work provides empirical evidence that gaseous CO_2 can be used to control pH in the enzymatic hydrolysis of urea under buffer-free conditions. By combining a mechanistic kinetic model with thermodynamic acid−base equilibria and gas−liquid mass transfer, a comprehensive reactor model was consolidated from literature that captures the strong coupling between reaction progress, pH evolution, and phase interactions. The modeling results clearly show that the intrinsic reaction pathway rapidly departs from the optimal pH range for urease activity if no means for pH control are applied, highlighting the necessity of active pH regulation. Controlled addition of CO_2 moderates this pathway by increasing DIC and shifting the system toward near-neutral conditions, thereby sustaining higher enzymatic activity and improving conversion.

Experimental validation confirmed that even modest CO_2 overpressures significantly enhance urea hydrolysis by lowering pH and stabilizing enzyme performance. Parameter estimation demonstrated good agreement between model predictions and experimental data, supporting the predictive capability of the framework. Furthermore, Bayesian optimization proved to be a robust tool for identifying optimal CO_2 partial pressures despite the nonlinear and nonsmooth nature of the coupled reaction−equilibrium system. While practical implementation requires careful estimation of mass transfer parameters and enzyme activity, the results establish the basis for CO_2-based pH control as a viable and scalable alternative to conventional buffering strategies. Overall, the combined modeling−experimental approach provides a powerful methodology for designing and optimizing enzymatic processes in which pH dynamics play a central role, while simultaneously reducing the need for additional chemicals and downstream processing. Based on the validated model, an extended control with time-dependent dosing can be pursued, taking into account the uncertainty of the model in difficult-to-estimate or changing parameters like k_La and f_{ac}. For this purpose, a stochastic model predictive control strategy has been developed on the basis of the current model and is reported in a separate publication.[34]

ASSOCIATED CONTENT

Data Availability Statement

The data and Python code underlying this study, as reported in the manuscript and the Supporting Information, are openly available in TORE at 10.15480/882.17011.

Supporting Information

The Supporting Information is available free of charge at https://pubs.acs.org/doi/10.1021/acs.iecr.6c00912.

Details on analytical methods and calibration, experimental ammonia, urea, and pH results, HPLC chromatograms, kinetic model parameter fitting, Bayesian optimization results, and experimental validation of the selected optimization points (PDF)

AUTHOR INFORMATION

Corresponding Authors

Leandros Paschalidis − *Institute of Process Systems Engineering, Hamburg University of Technology, 21073 Hamburg, Germany; United Nations University Hub on Engineering to Face Climate Change at the Hamburg University of Technology, United Nations University Institute for Water, Environment and Health (UNU-INWEH), 21073 Hamburg, Germany*; Email: leandros.paschalidis@tuhh.de

Andreas Liese − *Institute of Technical Biocatalysis, Hamburg University of Technology,, 21073 Hamburg, Germany; United Nations University Hub on Engineering to Face Climate Change at the Hamburg University of Technology, United Nations University Institute for Water, Environment and Health (UNU-INWEH), 21073 Hamburg, Germany*; orcid.org/0000-0002-4867-9935; Email: liese@tuhh.de

Mirko Skiborowski − *Institute of Process Systems Engineering, Hamburg University of Technology, 21073 Hamburg, Germany; United Nations University Hub on Engineering to Face Climate Change at the Hamburg University of Technology, United Nations University Institute for Water, Environment and Health (UNU-INWEH), 21073 Hamburg, Germany*; orcid.org/0000-0001-9694-963X; Email: mirko.skiborowski@tuhh.de

Authors

Kayla Reata Dittmer − *Institute of Technical Biocatalysis, Hamburg University of Technology,, 21073 Hamburg, Germany; United Nations University Hub on Engineering to Face Climate Change at the Hamburg University of Technology, United Nations University Institute for Water, Environment and Health (UNU-INWEH), 21073 Hamburg, Germany*

Chloe Ng-Brossard − *Institute of Technical Biocatalysis, Hamburg University of Technology,, 21073 Hamburg, Germany; United Nations University Hub on Engineering to Face Climate Change at the Hamburg University of Technology, United Nations University Institute for Water, Environment and Health (UNU-INWEH), 21073 Hamburg, Germany*

Daniel Ohde − *Institute of Technical Biocatalysis, Hamburg University of Technology,, 21073 Hamburg, Germany; United Nations University Hub on Engineering to Face Climate Change at the Hamburg University of Technology, United Nations University Institute for Water, Environment and Health (UNU-INWEH), 21073 Hamburg, Germany*

Complete contact information is available at: https://pubs.acs.org/10.1021/acs.iecr.6c00912

Author Contributions

K.R.D.: Writing—original draft, writing—review and editing, investigation, visualization, validation, formal analysis, data curation. L.P.: Writing—original draft, writing—review and editing, visualization, software, methodology, data curation, conceptualization. C.N.-B.: Investigation, writing—review and editing. D.O.: Writing—review and editing, supervision, project administration, funding acquisition. A.L.: Writing—review and editing, supervision, funding acquisition, conceptualization. M.S.: Writing—review and editing, supervision, project administration, funding acquisition, conceptualization.

Notes

The authors declare no competing financial interest.

https://doi.org/10.1021/acs.iecr.6c00912
Ind. Eng. Chem. Res. XXXX, XXX, XXX−XXX

■ ACKNOWLEDGMENTS

Financial support from the Collaborative Research Center (CRC) "SMART Reactors for Future Process Engineering," funded by the Deutsche Forschungsgemeinschaft (DFG, German Research Foundation) — project number 503850735—at the Hamburg University of Technology (TUHH), is gratefully acknowledged.

■ REFERENCES

(1) Jegannathan, K. R.; Nielsen, P. H. Environmental assessment of enzyme use in industrial production – a literature review. *J. Cleaner Prod.* **2013**, *42*, 228–240.
(2) Krajewska, B. Ureases I. Functional, catalytic and kinetic properties: A review. *J. Mol. Catal. B: Enzym.* **2009**, *59* (1–3), 9–21.
(3) Sahu, J. N.; Mahalik, K.; Patwardhan, A. V.; Meikap, B. C. Equilibrium and Kinetic Studies on the Hydrolysis of Urea for Ammonia Generation in a Semibatch Reactor. *Ind. Eng. Chem. Res.* **2008**, *47*, 4689–4696.
(4) Dixon, N. E.; Gazzola, C.; Blakeley, R. L.; Zerner, B. Jack bean urease (EC 3.5.1.5). Metalloenzyme. Simple biological role for nickel. *J. Am. Chem. Soc.* **1975**, *97* (14), 4131–4133.
(5) Dixon, N. E.; Hinds, J. A.; Fihelly, A. K.; Gazzola, C.; Winzor, D. J.; Blakeley, R. L.; Zerner, B. Jack bean urease (EC 3.5.1.5). IV. The molecular size and the mechanism of inhibition by hydroxamic acids. Spectrophotometric titration of enzymes with reversible inhibitors. *Can. J. Biochem.* **1980**, *58* (12), 1323–1334.
(6) Kappaun, K.; Piovesan, A. R.; Carlini, C. R.; Ligabue-Braun, R. Ureases: Historical aspects, catalytic, and non-catalytic properties — A review. *Journal of Advanced Research* **2018**, *13*, 3–17.
(7) Zhang, J.; Wang, Z.; He, C.; Liu, X.; Zhao, W.; Sun, S.; Zhao, C. Safe and Effective Removal of Urea by Urease-Immobilized, Carboxyl-Functionalized PES Beads with Good Reusability and Storage Stability. *ACS Omega* **2019**, *4* (2), 2470.
(8) Van Gelder, M. K.; Jong, J. A.; Folkertsma, L.; Guo, Y.; Blüchel, C.; Verhaar, M. C.; Odijk, M.; Van Nostrum, C. F.; Hennink, W. E.; Gerritsen, K. G. Urea removal strategies for dialysate regeneration in a wearable artificial kidney. *Biomaterials* **2020**, *234*, 119735.
(9) Botewad, S. N.; Gaikwad, D. K.; Girhe, N. B.; Thorat, H. N.; Pawar, P. P. Urea biosensors: A comprehensive review. *Biotechnol. Appl. Biochem.* **2023**, *70* (2), 485–501.
(10) Singh, S.; Sharma, M.; Singh, G. Recent advancements in urea biosensors for biomedical applications. *IET Nanobiotechnol.* **2021**, *15* (4), 358–379.
(11) Nicolau, E.; Fonseca, J. J.; Rodríguez-Martínez, J. A.; Richardson, T.-M. J.; Flynn, M.; Griebenow, K.; Cabrera, C. R. Evaluation of a Urea Bioelectrochemical System for Wastewater Treatment Processes. *ACS Sustainable Chem. Eng.* **2014**, *2* (4), 749–754.
(12) Urbańczyk, E.; Sowa, M.; Simka, W. Urea removal from aqueous solutions–a review. *J. Appl. Electrochem.* **2016**, *46* (10), 1011–1029.
(13) Sahin, B.; Ozbey-Unal, B.; Arslan, N.; Çiftçi, Y. Ö.; Keskinler, B.; Balcik, C. Pee-cycling: Boosting fertilizer potential of human urine using urease-immobilized polymeric high internal phase emulsion. *Resour., Conserv. Recycl.* **2025**, *215*, 108168.
(14) Yahya, M. N.; Gökçekuş, H.; Orhon, D.; Keskinler, B.; Karagunduz, A.; Omwene, P. I. A Study on the Hydrolysis of Urea Contained in Wastewater and Continuous Recovery of Ammonia by an Enzymatic Membrane Reactor. *Processes* **2021**, *9* (10), 1703.
(15) Qin, Y.; Cabral, J. M. S. Kinetic studies of the urease-catalyzed hydrolysis of urea in a buffer-free system. *Appl. Biochem. Biotechnol.* **1994**, *49*, 217–240.
(16) Hu, G.; Pojman, J. A.; Scott, S. K.; Wrobel, M. M.; Taylor, A. F. Base-Catalyzed Feedback in the Urea-Urease Reaction. *J. Phys. Chem. B* **2010**, *114* (44), 14059–14063.
(17) Li, W.; Li, Y.; Yang, Z.; Xu, C. pH Control in a Urease-catalyzed Reaction Using Weak-base Beads as Polymer-supported Buffer Agents. *Chem. Lett.* **2016**, *45* (8), 1027–1029.
(18) Hoshan, L.; Jiang, R.; Moroney, J.; Bui, A.; Zhang, X.; Hang, T.-C.; Xu, S. Effective bioreactor pH control using only sparging gases. *Biotechnol. Progress* **2019**, *35* (1), e2743.
(19) Xu, S.; Chen, H. High-density mammalian cell cultures in stirred-tank bioreactor without external pH control. *J. Biotechnol.* **2016**, *231*, 149–159.
(20) Paschalidis, L.; Beer, B.; Sutiono, S.; Sieber, V.; Burger, J. Design of enzymatic cascade reactors through multi-objective dynamic optimization. *Biochem. Eng. J.* **2022**, *181*, 108384.
(21) Paschalidis, L.; Fröschl, D.; Ibañez, M.; Sutiono, S.; Sieber, V.; Burger, J. Boosting of enzymatic cascades by intermediates: Theoretical analysis and model-based optimization. *Biochem. Eng. J.* **2024**, *210*, 109440.
(22) Zou, S.; Wang, D.; Xiao, J.; Feng, X. Mathematical Model for a Three-Phase Enzymatic Reaction System. *Ind. Eng. Chem. Res.* **2023**, *62* (10), 4337–4343.
(23) Hidalgo, A. M.; Sánchez, A.; Gómez, J. L.; Gómez, E.; Murcia, M. D. Kinetic Study of the Enzymatic Synthesis of 2-Phenylethyl Acetate in a Discontinuous Tank Reactor. *Ind. Eng. Chem. Res.* **2018**, *57* (33), 11280–11287.
(24) Moynihan, H. J.; Lee, C. K.; Clark, W.; Wang, N.-H. L. Urea hydrolysis by immobilized urease in a fixed-bed reactor: Analysis and kinetic parameter estimation. *Biotechnol. Bioeng.* **1989**, *34* (7), 951–963.
(25) Fidaleo, M.; Lavecchia, R. Kinetic study of enzymatic urea hydrolysis in the pH range 4–9. *Chem. Biochem. Eng. Q.* **2003**, *17* (4), 311–318.
(26) Petersen, V.; Markfoged, R.; Hafner, S. D.; Sommer, S. G. A new slurry pH model accounting for effects of ammonia and carbon dioxide volatilization on solution speciation. *Nutrient Cycling Agroecosystems* **2014**, *100*, 189–204.
(27) Daschakraborty, S.; Kiefer, P. M.; Miller, Y.; Motro, Y.; Pines, D.; Pines, E.; Hynes, J. T. Reaction Mechanism for Direct Proton Transfer from Carbonic Acid to a Strong Base in Aqueous Solution I: Acid and Base Coordinate and Charge Dynamics. *J. Phys. Chem. B* **2016**, *120*, 2271–2280.
(28) Carpenter, W. B.; Fournier, J. A.; Lewis, N. H. C.; Tokmakoff, A. Picosecond Proton Transfer Kinetics in Water Revealed with Ultrafast IR Spectroscopy. *J. Phys. Chem. B* **2018**, *122*, 2792–2802.
(29) Schlipköter, K. E.; Betke, T.; Kleber, J.; Gröger, H.; Liese, A. Fatty alcohol synthesis from fatty acids at mild temperature by subsequent enzymatic esterification and metal-catalyzed hydrogenation. *Org. Biomol. Chem.* **2020**, *18* (39), 7862–7867.
(30) Analysis of urea: Fast, reproducible HPLC method. English. Tech. rep. APP-A-111. Leland, NC, USA: MicroSolv Technology Corporation, 2010, https://www.mtcusa.com/images/MICROSOLV/kb-images/2020/10/No-111-Analysis-of-Urea-1.pdf (visited on 09/02/2026).
(31) Walther, D.; Ruben, M.; Rau, S. Carbon dioxide and metal centres: from reactions inspired by nature to reactions in compressed carbon dioxide as solvent. *Coord. Chem. Rev.* **1999**, *182* (1), 67–100.
(32) Maithani, S.; Pal, M.; Maity, A.; Pradhan, M. Isotope selective activation: a new insight into the catalytic activity of urease. *RSC Adv.* **2017**, *7* (50), 31372–31376.
(33) Krajewska, B.; Zaborska, W. The effect of phosphate buffer in the range of pH 5.80–8.07 on jack bean urease activity. *J. Mol. Catal. B: Enzym.* **1999**, *6* (1), 75–81.
(34) Santra, S.; Paschalidis, L.; Skiborowski, M.; Faulwasser, T. CO2-Driven pH Control in the Enzymatic Hydrolysis of Urea: A Framework for Stochastic Model Predictive Control *Ind. Eng. Chem. Res.* 2026. (submitted).

https://doi.org/10.1021/acs.iecr.6c00912
Ind. Eng. Chem. Res. XXXX, XXX, XXX–XXX